The morphology of the topside ionosphere of Mars under different solar wind conditions: Results of a multi-instrument observing campaign by Mars Express in 2010

Paul Withers [a,b,*], M. Matta [b], M. Lester [c], D. Andrews [d], N. J. T. Edberg [d], H. Nilsson [d], H. Opgenoorth [d], S. Curry [e], R. Lillis [e], E. Dubinin [f], M. Fränz [f], X. Han [g], W. Kofman [h], L. Lei [i], D. Morgan [j], M. Pätzold [k], K. Peter [k], A. Opitz [ℓ], J. A. Wild [m], O. Witasse [n]

[a] *Department of Astronomy, Boston University, 725 Commonwealth Avenue, Boston, MA 02215, USA*

[b] *Center for Space Physics, Boston University, 725 Commonwealth Avenue, Boston, MA 02215, USA*

[c] *University of Leicester, Leicester, United Kingdom*

[d] *Swedish Institute for Space Physics, IRF, Sweden*

[e] *University of California, Berkeley, United States*

[f] *Max Planck Institute for Solar System Research, Germany*

[g] *Key Laboratory of Earth and Planetary Physics, Institute of Geology and Geophysics, Chinese Academy of Sciences, Beijing 100029, China*

[h] *Institut de Planetologie et dAstrophysique de Grenoble, CNRS/UGA, 53, 38041*

Preprint submitted to Planetary and Space Science *22 September 2015*

Grenoble Cedex 9, France and Visiting Professor at Space Research Centre of the Polish Academy of Sciences, Warsaw, Poland

[i] *NSSC, Beijing, China*

[j] *University of Iowa, Iowa City, United States*

[k] *Rheinisches Institut für Umweltforschung an der Universität zu Köln, Abt. Planetenforschung, Köln, Germany*

[ℓ] *ESTEC, Noordwijk, The Netherlands*

[m] *Physics Department, Lancaster University, Lancaster, LA1 4YB, United Kingdom*

[n] *Scientific Support Office, European Space Agency, Noordwijk, The Netherlands*

Abstract

Since the internally-generated magnetic field of Mars is weak, strong coupling is expected between the solar wind, planetary magnetosphere, and planetary ionosphere. However, few previous observational studies of this coupling incorporated data that extended from the solar wind to deep into the ionosphere. Here we use solar wind, magnetosphere, and ionosphere data obtained by the Mars Express spacecraft during March/April 2010 to investigate this coupling. We focus on three case studies, each centered on a pair of ionospheric electron density profiles measured by radio occultations, where the two profiles in each pair were obtained from the same location at an interval of only a few days. We find that high dynamic pressures in the solar wind are associated with compression of the magnetosphere, heating of the magnetosheath, reduction in the vertical extent of the ionosphere, and abrupt changes in electron density at the top of the ionosphere. The first three of these associations are analogous to the behavior of the plasma environment of Venus, but the final one is not. These results reinforce the notion that changes in solar forc-

ing influence the behaviors of all of the tightly coupled regions within the Martian plasma environment.

Key words: Mars, solar wind, magnetosphere, ionosphere

1 Introduction

Due to differences in planetary size, rotation rate, magnetic moment, and heliocentric distance, there is great diversity amongst the plasma environments of solar system bodies (Cravens, 2004; Witasse et al., 2008; Schunk and Nagy, 2009). Mars (Nagy et al., 2004; Russell, 2006) and Venus (Brace and Kliore, 1991; Luhmann et al., 1992), which lack significant internal magnetic fields, are characterized by induced magnetospheres formed through interactions between the upper atmosphere of the planet and the impinging solar wind plasma. An analogous process is also known to occur at Saturn's largest moon, Titan (Cravens et al., 2010; Luhmann et al., 2012).

The Martian system is particularly interesting because it contains a varied mixture of magnetic environments. This is caused by the presence of strong, spatially inhomogeneous, crustal magnetic field patches and the absence of any dipolar magnetic field produced in the planet's interior (Acuña et al., 1999). Magnetic field strength, local field direction and connectivity to the solar wind all vary on length scales that are less than a tenth of the planet's radius, circumstances that are not found anywhere else in the solar system.

The effects of the solar wind on the upper atmosphere of Mars are modu-

* Corresponding author
Email address: withers@bu.edu (Paul Withers).

lated by the intervening induced magnetosphere (Nagy et al., 2004; Russell, 2006). Many of the major features of ion outflow from the planet and plasma heating in the upper atmosphere are intricately coupled to the intensity and geometry of the draped field within the induced magnetosphere, conditions that are determined by solar wind dynamic pressure and orientation of the interplanetary magnetic field. The conditions in the impinging solar wind are hence highly important for governing the dynamics of the solar wind's interaction with the Martian upper atmosphere, as the induced magnetosphere it generates is constantly evolving in response to solar wind variations.

To date, the goal of obtaining a comprehensive understanding of how the ionosphere of Mars is affected by the solar wind has been impeded by the lack of appropriate and simultaneous information on the solar wind, magnetosphere, and ionosphere. In order to overcome this problem, we arranged for three dedicated campaigns of coordinated observations by several MEX instruments during the periods of March/April 2010, March/April 2012, and spring 2014. The objective of this paper is to investigate how the structure of the topside of the Martian ionosphere was influenced by solar wind and magnetospheric conditions during the first of these campaigns; the large-scale results of the observing campaigns will be reported elsewhere.

Mars was near opposition during these time intervals, and hence it was possible to infer solar wind conditions at Mars from observations closer to the Sun, such as data from the ACE, STEREO, Cluster, and THEMIS spacecraft. The MEX datasets selected for study are ionospheric electron density profiles obtained by MaRS, the Mars Express Radio Science Experiment, in situ electron densities measured by the MARSIS radar sounder, and in situ magnetospheric and solar wind conditions seen by ASPERA.

In the context of this work, the topside ionosphere is the region above about 180 km altitude. Transport processes are important in the topside ionosphere, but not at lower altitudes. Ions are produced by photoionization and, to a lesser degree, by impact ionization due to the precipitation of charged particles into the neutral atmosphere. The topside ionosphere is thought to be predominantly a mixture of O^+ and O_2^+ ions, though its composition is poorly-constrained by observations. Electron densities in the topside ionosphere generally decrease with increasing altitude, but a range of vertical structures is possible (Withers et al., 2012).

In Section 2, we discuss the expected response of the plasma environment of Mars to changes in the solar wind. In Section 3, we establish the overarching solar wind and magnetospheric conditions that pertain to the March/April 2010 campaign. In Section 4, we introduce observations of the ionosphere by radio occultations (Section 4.1) and local radar sounding (Section 4.2) that are relevant to our three case studies. In Section 5, we synthesize observations spanning the upstream solar wind, the magnetosphere, and the ionosphere for the three case studies. In Section 6, we summarize our conclusions.

2 Expected response of the plasma environment of Mars to changes in the dynamic pressure of the solar wind

The plasma environment of Mars, which encompasses the planet's magnetosphere and ionosphere, has been reviewed by Nagy et al. (2004), Brain (2006), and Withers (2009). Here we summarize some of its key features. Upstream of the bow shock (typical subsolar altitude, 2000 km), the plasma population is the undisturbed solar wind: supersonic, cool, and low density. The magne-

tosheath lies inside the bow shock. Plasma in the magnetosheath originated from the solar wind, but is subsonic, hotter, more dense, and more turbulent. The inner boundary of the magnetosheath is the "magnetic pileup boundary" (MPB), which typically occurs at an altitude of 850 km (subsolar point). "The MPB clearly separates two very different regions: a magnetosheath with low amplitude and turbulent magnetic fields and a region of high pile-up fields, the Magnetic Pile-up Region (MPR), where the solar wind is piled-up and draped around the ionosphere" (Nagy et al., 2004). Within the MPR, the plasma composition is dominated by planetary ions, unlike the proton-dominated solar wind. However, the electron population within the MPR is of solar wind origin (Mitchell et al., 2001). The inner boundary of the MPR is the "photoelectron boundary" (PEB), which typically occurs at an altitude of 400 km. As explained by Mitchell et al. (2001), "Above the boundary, electron energy spectra are consistent with solar wind electrons that have been shocked and then modified by impact with exospheric neutrals (Crider et al., 2000). Below the boundary, electron energy spectra exhibit a broad feature from 20 to 50 eV, which likely results from a blend of unresolved photoionization peaks that have been predicted by published models of ionospheric photoelectrons at Mars (Fox and Dalgarno, 1979; Mantas and Hanson, 1979). A second feature at $\sim$500 eV results from oxygen Auger electrons (Mitchell et al., 2000)." Below the PEB, electrons and ions are derived from the ionization, primarily by photoionization, of neutral atmospheric species. This region is the ionosphere. The upper boundary of the ionosphere is sometimes very sharp. Duru et al. (2009) analyzed in situ electron densities measured as a novel and unexpected byproduct of the MARSIS radar sounder. They reported very sharp gradients in electron density in which electron densities dropped to very low values in about 18% of the orbits studied. Where these sharp gradients occur,

we assume that they coincide with the PEB.

Previous work on the effects of high dynamic pressure in the solar wind on the plasma environment of Mars has used MGS MAG/ER, MEX ASPERA, and MEX MARSIS to show that high dynamic pressure compresses the magnetic pileup boundary (Crider et al., 2003; Dubinin et al., 2006; Opgenoorth et al., 2013) and has used MGS MAG/ER to show that high dynamic pressure compresses the photoelectron boundary (Crider et al., 2003; Brain, 2006), Escape rates are also enhanced by high solar wind dynamic pressure (Lundin et al., 2008; Nilsson et al., 2010; Edberg et al., 2009, 2010; Kaneda et al., 2007).

Not known from observations are the effects of the dynamic pressure of the solar wind on either the altitude and occurrence probability of the abrupt changes in electron density observed by MARSIS or the vertical structure of the topside ionosphere as observed by radio occultations. However, numerical simulations have started to investigate this topic. In a series of magnetohydrodynamic simulations, Ma et al. (2014) found that the altitude of the top of the ionosphere (defined in this case by a density of 100 cm^{-3}) did not change during a period of high dynamic pressure, but did rise by several hundred kilometers upon return to normal dynamic pressures at the end of the compression phase. The recovery timescale was more than one hour. They also reported that the topside electron density profile was characterized by large fluctuations with altitude during, but not after, the period of high dynamic pressure. In the context of this work, such density profiles are said to be "disturbed".

Analogy to Venus, which is also a non-magnetized planet and whose plasma environment was studied comprehensively by the Pioneer Venus Orbiter mission, is useful for setting expectations concerning the response of the plasma

environment of Mars to changes in the dynamic pressure of the solar wind. On Venus, many plasma properties, including ion and electron temperatures and densities and the direction and magnitude of the magnetic field, change abruptly at a boundary called the ionopause (Brace et al., 1983). The ionopause, which occurs at 200–1000 km altitude, is a pressure boundary as here "the kinetic pressure of the ionospheric plasma is approximately equal to the dynamic pressure of the unperturbed solar wind. On the dayside the solar wind dynamic pressure is transformed to magnetic pressure between the bow shock and the ionopause." (Schunk and Nagy, 2009). When the solar wind dynamic pressure is low relative to the ionospheric thermal pressure, the ionopause is narrow and clear and its altitude is high. When the solar wind dynamic pressure is relatively high, ionospheric thermal pressure alone is not sufficient to balance it and the ionosphere becomes magnetized with large-scale horizontal fields. At these times, the ionopause is broad and less distinctive, and its altitude is lower (Brace et al., 1983; Russell and Vaisberg, 1983; Nagy et al., 2004).

It has been suggested that, under typical conditions at Mars, the ionospheric thermal pressure is not sufficient to balance the solar wind dynamic pressure (Zhang et al., 1990) and a sharp, high altitude ionopause and an unmagnetized ionosphere are not expected. However, later work by these authors (Zhang and Luhmann, 1992) re-evaluated those results and concluded that solar wind-ionosphere pressure balance at Mars ought to be Venus-like. Duru et al. (2009) interpreted occasional occurrences of very sharp gradients in electron density as being analogous to the narrow and clear ionopause seen at Venus for low solar wind pressures.

A long-standing, overarching goal in the field of Mars plasma science is to

understand the effects of the dynamic pressure of the solar wind on the end-to-end state of the entire plasma environment of Mars. The objective of this paper, to investigate how the structure of the topside of the Martian ionosphere is influenced by solar wind and magnetospheric conditions, therefore addresses a neglected aspect of the overarching goal. Analogy with Venus suggests that periods of high dynamic pressure in the solar wind will be associated with compressed bow shock and magnetic pileup boundary distances, lower altitudes of the photoelectron boundary, the absence of abrupt changes (idealized ionopauses) in electron densities, and undisturbed topside electron density profiles.

3 Solar wind and magnetospheric conditions during the March/April 2010 campaign

In order to highlight the effects of temporal variations, rather than spatial variations associated with the unique magnetic morphology of Mars, we focus on case studies for which multiple ionospheric profiles are available from a location that is practically fixed. Three such case studies are possible for the March/April 2010 campaign. For the March/April 2012 campaign, infelicitous orbital geometry precluded radio occultations. The spring 2014 campaign was conducted after the project reported on in this article was completed. The precise dates and locations of the three case studies from the March/April 2010 campaign will be discussed in Section 4.

Figure 1 illustrates the positions of Earth and Mars on 1 April 2010, when the Earth-Sun-Mars angle was approximately 30 degrees. Given this geometry, solar wind data from both Earth and STEREO-B are reasonably suitable

for extrapolating conditions in the solar wind, which flows radially outwards from the Sun, to Mars. Since Earth and Mars were on the same branch of the Parker spiral during March/April 2010, any solar energetic particle events that impacted Earth in this period should also have impacted Mars. The ionizing solar irradiance was low during this period, with the value of F10.7 at 1 AU being between 70 and 90 units from 1 March 2010 to 30 April 2010.

Figure 2 illustrates the geometry of the MEX orbit in 7 March and 15 April 2010. It also indicates the predicted positions of the bow shock and the magnetic pileup boundary (Vignes et al., 2000). The orbital period is 7 hours. Since apoapsis is sunward of the nominal location of the bow shock, MEX spends a considerable time in the solar wind on most orbits. Under these circumstances, ASPERA can measure solar wind density, speed, and dynamic pressure (Barabash et al., 2004, 2006). Time series of the solar wind dynamic pressure measured at Mars by ASPERA during March and April 2010 are shown in Figure 3. Also shown is an estimate of the dynamic pressure based on extrapolation to Mars of measurements at STEREO-B (Opitz et al., 2009, 2010). Extrapolations were made using data from STEREO-A, STEREO-B, and the OMNIWeb suite of near-Earth assets. Since the extrapolation based on STEREO-B data agreed best with the ASPERA data, only that extrapolation is shown. The ASPERA and STEREO-B-derived dynamic pressures do not agree perfectly, although there is qualitative agreement when conditions are relatively simple. Neither source should be expected to be definitive. ASPERA was not designed as a solar wind monitor and its inferred solar wind properties ought to be treated cautiously. Similarly, the STEREO-B extrapolations are extrapolations, not observations. The subsequent text discusses estimated solar wind conditions from both these sources when interpreting

magnetospheric and ionospheric observations in the context of the individual case studies.

ASPERA also observed magnetospheric conditions during the March/April 2010 campaign. During this interval, MEX entered the Martian magnetosheath in the southern tail, continued into the nightside upper ionosphere before reaching periapsis near the northern dawn flank terminator region and finally exited through the magnetosheath on the dayside dusk flank, returning back into the upstream solar wind (Figure 2). The configuration of the orbit changed slowly from one orbit to the next. The altitudes of the magnetic pileup boundary and photoelectron boundary as encountered by MEX during March/April 2010 (Dubinin et al., 2006) are shown in Figure 4. Since they are on the dayside, the outbound altitudes are more relevant for this study than the inbound altitudes. These magnetospheric conditions will be discussed subsequently in the context of the individual case studies.

4 Ionospheric conditions

4.1 Radio occultation profiles

Six vertical profiles of ionospheric electron density acquired by the Mars Express Radio Science Experiment, MaRS (Pätzold et al., 2004; Pätzold and thirty colleagues, 2009), during March/April 2010 are important for this work. These extend from ∼60 km to above 800 km altitude with a vertical resolution of 0.5 km and a measurement uncertainty that is on the order of $0.5-1.0$ x 10^3 cm^{-3}. The locations of these six profiles are shown in Figure 5. They can be grouped into three pairs of profiles that have similar locations. Case study A

focuses on the profiles acquired on 8 March (orbit 7919) and 21 March (orbit 7964), case study B on 8 April (orbit 8027) and 10 April (8034), and case study C on 15 April (orbit 8051) and 17 April (8058). Each pair is well-suited to studies of the effects of solar wind-magnetosphere-ionosphere coupling, since their similar locations eliminate a host of possible causes of variability in ionospheric profiles. The two profiles in pair A, orbits 7919/7964, are separated by 13 days, whereas the profiles in pairs B and C, orbits 8027/8034 and 8051/8058, respectively are each separated by a mere two days. Table 1 lists the dates, times, locations, and solar zenith angles (SZAs) of these six profiles. The SZAs of these profiles are within 3 degrees of the ground-level terminator at 90°, but the sun does not set at ionospheric altitudes until much greater SZAs (105° at 120 km). Thus the physical processes governing these ionospheric profiles are effectively those of the dayside ionosphere, albeit with the addition of possible trans-terminator flow. Figure 6 directly compares the two profiles in each pair, which were smoothed using the algorithm described by Peter et al. (2014). Solar zenith angle variations and seasonal/latitude/longitude variations in the neutral atmosphere are too small to be plausible causes of any significant differences in the topside ionosphere between the two profiles in a pair.

The two profiles that comprise pair A, acquired on 8 March and 21 March, have distinctly different topside ionospheric structures (Figure 6). Above the main peak, electron densities decrease with increasing altitude above the main peak in both profiles. However, large fluctuations in electron density are present above 200 km on 8 March, but only above 350 km on 21 March. Variations in crustal magnetic field properties cannot be responsible for these differences, for they are weak at this geographic location, as shown in Figure 5. The only

remaining plausible cause for the dramatic difference in topside ionospheric conditions is variation in solar wind and magnetospheric conditions from 8 to 21 March 2010. Statistical studies using the MGS Electron Reflectometer (ER) have shown that magnetic fieldlines at this latitude and longitude, 400 km, and near-terminator solar zenith angles (90°–116°) have a ∼40% likelihood of being open and a similar likelihood of being draped, with only a ∼10% likelihood of being closed (Brain et al., 2007; Lillis and Brain, 2013).

The two profiles that comprise pair B, acquired on 8 April and 10 April, have very similar topside ionospheric structures (Figure 6). Again, the crustal magnetic field is weak at the locations of these two profiles (Figure 5). Magnetic fieldlines here have a ∼55% likelihood of being open, a ∼35% likelihood of being draped, and only a ∼5% likelihood of being closed (Brain et al., 2007; Lillis and Brain, 2013).

The two profiles that comprise pair C, acquired on 15 April and 17 April, have distinctly different topside ionospheric structures (Figure 6). At altitudes above 300 km, electron densities are much greater on 17 April than on 15 April. Here the crustal magnetic field is relatively strong, near 100 nT at 150 km altitude (Figure 5). Despite the small geographic separation between these two profiles, their magnetic topologies differ significantly. Magnetic fieldlines at the latitude and longitude of the profile from 15 April have a ∼10% likelihood of being open, a ∼40% likelihood of being draped, and a ∼40% chance of being closed. The closed instances are dominated by trapped plasma, not plasma voids (Brain et al., 2007; Lillis and Brain, 2013). Magnetic fieldlines at the latitude and longitude of the profile from 17 April have a negligible likelihood of being open, a ∼80% likelihood of being draped, and a ∼20% chance of being closed. The closed instances are dominated by plasma voids,

not trapped plasma (Brain et al., 2007; Lillis and Brain, 2013).

4.2 MARSIS local electron densities

The MARSIS radar sounder conducted ionospheric sounding around periapsis on many orbits during the March/April 2010 campaign (Gurnett et al., 2005, 2008). Time series of local electron densities at the spacecraft were also obtained around periapsis on these orbits (Duru et al., 2008) and abrupt changes in dayside local electron density were observed on many of these orbits. Figure 7 shows the orbits on which these abrupt changes were detected and the corresponding altitudes. Figure 7 also provides a binary classification of the abruptness of the change in electron density. "More abrupt" changes are those that Duru et al. (2009) would have classified as an "ionopause" (density changes from >500 cm^{-3} to <200 cm^{-3} with a rate of change that exceeds 50 cm^{-3} per 7.54 seconds, the instrumental cadence).

During the March/April 2010 campaign, periapsis was near the terminator and at mid-northern latitudes (note that periapsis longitude varied from orbit to orbit due to the rotation of the planet beneath the orbital path of the spacecraft). Consequently, periapsis was far from the strongly-magnetized regions of the southern hemisphere, and also far from the locations of the radio occultation electron density profiles. Comparisons between MaRS radio occultation observations and MARSIS observations are complicated by the substantial distance between them. However, this problem is not insurmountable as the interaction of the solar wind with Mars occurs on a global, not local, scale. If the solar wind dynamic pressure is high at one location, then it will be high at the other location as well. As long as crustal magnetic fields are weak at

both locations, which is true for case studies A and B, then the ionospheric response should be grossly similar at both locations.

5 Analysis

Having introduced the datasets to be used in this investigation, we next synthesize the ionospheric, magnetospheric, and solar wind observations relevant for each case study in turn.

5.1 Case study A: 8 March and 21 March

Preceding figures showed observations of the solar wind, magnetic pileup boundary, photoelectron boundary, and ionopause over the entire span of this campaign. Figure 8 shows a subset of these observations relevant for the time of this case study.

The topside ionosphere in the MEX radio occultation profile from 8 March (orbit 7919) has an unusual structure that is highly disturbed. The fluctuations in the topside electron densities are larger than the experimental noise and have a longer vertical correlation length than the noise-induced point-to-point fluctuations in the other profiles. The transition at 200 km from a region of smoothly decreasing electron densities to a region of fluctuating electron densities is associated with a change in the scale height of the background ionosphere. By contrast, electron densities from 21 March (orbit 7964) decrease with increasing altitude to 350 km without large fluctuations. We note that electron densities in the low-altitude M1 layer are greater on 8 March (orbit 7919) than 21 March (orbit 7964), but neglect this to focus on the topside.

Between 6 March and 11 March, MARSIS data are only available for orbit 7918 (7 March), which has a striking ionopause at the relatively low altitude of 567 km. Here electron densities decreased by a factor of 50 with an effective scale height of 5 km, which makes it an extremely clear example of a MARSIS ionopause detection. MARSIS data are available for orbit 7964 (21 March) and five other orbits between 20 March and 22 March (orbits 7961, 7962, 7965, 7968, and 7970). An ionopause was identified on 20 March (orbit 7961), again at a relatively low altitude (583 km), and a weaker abrupt change in local electron density was detected on the same date (orbit 7962, 610 km). Electron densities decreased by factors of 25 and 10 with effective scale heights of 10 km and 6 km on orbits 7961 and 7962, respectively. No abrupt change was detected on orbit 7964 (21 March).

The outbound photoelectron boundary and magnetic pileup boundary were unusually low around 8 March, being below 400 km and 700 km, respectively, on the outbound leg on 7–8 March. Both boundaries occurred at higher altitudes around 21 March. The solar wind dynamic pressure at Mars was high on 8 March, according to ASPERA measurements. High dynamic pressures are also predicted at around this time by extrapolation from STEREO-B. By contrast, the solar wind dynamic pressure was low on 21 March.

We interpret these diverse measurements as follows. High dynamic pressure in the solar wind on 7–8 March compressed the ionosphere, resulting in an ionopause detection at relatively low altitudes in MARSIS local electron density data (orbit 7918) and in the restriction of undisturbed ionospheric electron densities to altitudes less than 200 km in MEX radio occultation data (orbit 7919), similar to the simulations of Ma et al. (2014). A minor event on 20 March caused abrupt changes in MARSIS local electron densities, but did not

depress the altitudes of the outbound photoelectron boundary and magnetic pileup boundary significantly. According to the time series of solar wind dynamic pressure based on extrapolation from STEREO-B, a small localized maximum occurred on this date above a background of low dynamic pressures that spanned the surrounding week. However, no such event is readily identifiable in the ASPERA-derived solar wind dynamic pressures. Conditions had returned to normal by the time of the MEX radio occultation on 21 March.

5.2 Case study B: 8 April and 10 April

Figure 9 shows observations of the solar wind, magnetic pileup boundary, photoelectron boundary, and ionopause relevant for the time of this case study.

The topside ionospheres in the MEX radio occultation profiles from 8 April (orbit 8027) and 10 April (orbit 8034) are similar to each other. In both profiles, electron densities decrease with increasing altitude without large, long wavelength fluctuations, reaching the noise threshold of 2×10^2 cm^{-3} above 500 km. Neither profile contains regions of disturbed plasma analogous to those seen at high altitudes on 8 March.

Between 2 April and 12 April (orbits 8007 and 8040), MARSIS data are available for ten orbits. No abrupt changes in electron density were detected in MARSIS data from these ten orbits. Close to orbits 8027 (8 April) and 8034 (10 April), only orbits 8021, 8028, and 8035 have MARSIS data.

The outbound magnetic pileup boundary was above 1000 km on 8–10 April. The outbound photoelectron boundary was around 500 km at the time of the MEX radio occultation profile on 8 April and relatively high, around 1000

km on 9 and 11 April, though it was not detected by ASPERA on any orbits on 10 April. The only major coronal mass ejection (CME) event to impact Mars in March/April 2010 did so on 6 April (during orbit 8020). This event was previously discussed by Opgenoorth et al. (2013), who labeled it as their "Event 3". Accelerated ionospheric ions were observed by ASPERA for several orbits. However, the magnetosphere returned to a more quiescent state by 8 April (orbit 8027) and remained so until after 10 April. Solar wind dynamic pressures at Mars around 8–10 April were slightly, but not tremendously, elevated above the quiescent values seen in late March.

We interpret these diverse measurements as follows. The arrival of a CME at Mars on 6 April (orbit 8020) greatly disturbed the magnetosphere, yet no abrupt change in MARSIS local electron density data was present on the following orbit. The quieter solar wind conditions on 8–10 April did not produce any abrupt changes in MARSIS local electron density data (orbits 8028 and 8035) or unusual behavior in topside electron densities in MEX radio occultation data (orbits 8027 and 8034).

5.3 Case study C: 15 April and 17 April

Figure 10 shows observations of the solar wind, magnetic pileup boundary, photoelectron boundary, and ionopause relevant for the time of this case study.

Although electron densities in the MEX radio occultation profiles from 15 April (orbit 8051) and 17 April (orbit 8058) are similar at 200 km, they diverge significantly at higher altitudes. The average density at 350–450 km is less than 250 cm^{-3} on 15 April, but nearly 1500 cm^{-3} on 17 April. The ratio of these

two averages is greater than 6, whereas similar ratios for the other two case studies are less than 2. The 15 April occultation is the only one of these six for which the average density at 350–450 km is less than 500 cm^{-3}. Clearly, high altitude densities are unusually low on 15 April. In addition, the 17 April occultation is the only one of these six for which the average density at 350–450 km is greater than 1000 cm^{-3} (Duru et al., 2008; Andrews et al., 2013). The local magnetic topology may affect this comparison, since it differs between the locations of these two occultations (Section 4.1).

Between 12 April (orbit 8040) and 24 April (orbit 8080), MARSIS data are available for six orbits (8051, 8056, 8059, 8066, 8073, 8080). The only abrupt change in electron density from these six orbits occurred on 15 April (orbit 8051, 687 km). Electron densities decreased by an order of magnitude over a vertical distance of 30 km, which can be interpreted as implying an effective scale height of 15 km. This is sufficiently extreme that Duru et al. (2009) would classify it as an ionopause.

The altitudes of the outbound photoelectron boundary and magnetic pileup boundary were normal (∼600 km and ∼800 km, respectively) on 15 and 17 April. Magnetospheric conditions were rather dynamic around 15–17 April. Relative to surrounding orbits, the magnetosphere was compressed and the magnetosheath density was enhanced on orbit 8051 (15 April). Compression and sheath heating were also present on orbits 8054 (16 April) and 8057 (17 April) (no data from orbits 8055 and 8056), but orbit 8058 (17 April) corresponds to a short-lived period of relaxation. A short-lived period of high solar wind dynamic pressure was experienced early on 15 April with smaller, more typical dynamic pressures prevalent on 17 April.

We interpret these diverse measurements as follows. Multiple intervals of magnetospheric compression and heating, and associated relaxations, occurred around 15–17 April. Orbit 8051 on 15 April is best characterized as a period of compression and orbit 8058 on 17 April as a period of relaxation. The compression on orbit 8051 was strong enough to produce an abrupt change in MARSIS local electron density data and to lessen topside densities in MEX radio occultation data. More relaxed conditions did not produce an abrupt change in MARSIS local electron density data on orbits 8056 and 8059. However, they did cause topside electron densities in MEX radio occultation data on orbit 8058 to be larger than usual, similar to the simulations of Ma et al. (2014).

6 Conclusions

The dynamic solar wind influences conditions in the magnetosphere and ionosphere of Mars. High dynamic pressures in the solar wind lead to compression of the magnetosphere, heating in the magnetosheath, reduction in the vertical extent of the ionosphere, and abrupt changes in electron density at the top of the ionosphere. In some instances, these abrupt changes in electron density are sufficiently extreme that Duru et al. (2009) would classify them as ionopauses.

Most of these responses to high dynamic pressures in the solar wind are consistent with those seen at Venus. However, analogy with Venus would suggest that abrupt changes in local electron density (idealized ionopauses) should be absent during periods of high dynamic pressure. In fact, the opposite trend is suggested at Mars by these three case studies. Even so, this is such a small sample size that the results should not be accepted as definitive. Surveys of

ionopauses in MARSIS local electron density observations have not yet investigated whether their occurrences and physical properties are correlated with solar wind conditions (Duru et al., 2009), yet doing so would be valuable for firmly establishing whether this aspect of the Martian response to high dynamic pressures in the solar wind exhibits Venus-like or anti-Venus-like behavior. This would then lead to better understanding of the physical mechanisms that produce these distinct features and whether their observable characteristics are in any way diagnostic of important properties of the broader plasma environment.

The findings of this work reinforce the notion that different regions within the Martian plasma environment are tightly coupled, rather than being isolated entities. Variations in the population of charged particles emanating from the Sun can influence the Martian plasma environment all the way down to the topside ionosphere.

Acknowledgments

This work was stimulated by the meetings of the International Space Science Institute (ISSI) International Team "The induced magnetosphere of Mars: Physical processes and consequences". We gratefully acknowledge ISSI for support and hospitality, the Mars Express project for conducting dedicated observing campaigns, the STEREO team for making their data publicly available, Dave Brain for access to field topology maps, and an anonymous reviewer for helpful comments. PW acknowledges funding from NASA award NNX12AJ39G. DJA, NJTE, and HJO acknowledge funding from the Swedish National Space Board (SNSB). ML acknowledges support from STFC with

grant ST/K001000/1. AO acknowledges support from the Research Fellowship program at ESA ESTEC. The Mars Express Radio Science Experiment (MaRS) is funded by the German Space Agency (DLR) under Grant 50QM1401.

References

Acuña, M. H., Connerney, J. E. P., Ness, N. F., Lin, R. P., Mitchell, D., Carlson, C. W., McFadden, J., Anderson, K. A., Rème, H., Mazelle, C., Vignes, D., Wasilewski, P., Cloutier, P., 1999. Global distribution of crustal magnetization discovered by the Mars Global Surveyor MAG/ER Experiment. Science 284, 790–793.

Andrews, D. J., Opgenoorth, H. J., Edberg, N. J. T., André, M., Fränz, M., Dubinin, E., Duru, F., Morgan, D., Witasse, O., 2013. Determination of local plasma densities with the MARSIS radar: Asymmetries in the high-altitude Martian ionosphere. J. Geophys. Res. 118, 6228–6242.

Arkani-Hamed, J., 2004. A coherent model of the crustal magnetic field of Mars. J. Geophys. Res. 109, E09005, 10.1029/2004JE002265.

Barabash, S., Lundin, R., Andersson, H., Brinkfeldt, K., Grigoriev, A., Gunell, H., Holmström, M., Yamauchi, M., Asamura, K., Bochsler, P., Wurz, P., Cerulli-Irelli, R., Mura, A., Milillo, A., Maggi, M., Orsini, S., Coates, A. J., Linder, D. R., Kataria, D. O., Curtis, C. C., Hsieh, K. C., Sandel, B. R., Frahm, R. A., Sharber, J. R., Winningham, J. D., Grande, M., Kallio, E., Koskinen, H., Riihelä, P., Schmidt, W., Säles, T., Kozyra, J. U., Krupp, N., Woch, J., Livi, S., Luhmann, J. G., McKenna-Lawlor, S., Roelof, E. C., Williams, D. J., Sauvaud, J.-A., Fedorov, A., Thocaven, J.-J., 2006. The Analyzer of Space Plasmas and Energetic Atoms (ASPERA-3) for the Mars Express Mission. Space Sci. Rev. 126, 113–164.

Barabash, S., Lundin, R., Andersson, H., Gomholt, J., Holmström, M., Norberg, O., Yamauchi, M., Asamura, K., Coates, A. J., Linder, D. R., Kataria, D. O., Curtis, C. C., Hsieh, K. C., Sandel, B. R., Fedorov, A., Grigoriev, A., Budnik, E., Grande, M., Carter, M., Reading, D. H., Koskinen, H., Kallio, E., Riihelä, P., Säles, T., Kozyra, J. U., Krupp, N., Livi, S., Woch, J., Luhmann, J. G., McKenna-Lawlor, S., Orsini, S., Cerulli-Irelli, R. and-Maggi, M., Morbidini, A., Mura, A., Milillo, A., Roelof, E. C., Williams, D. J., Sauvaud, J.-A., Thocaven, J.-J., Moreau, T., Winningham, J. D., Frahm, R. A., Scherrer, J.and Sharber, J. R., Wurz, P., Bochsler, P., 2004. MaRS: Mars Express Orbiter Radio Science. ESA SP-1240: Mars Express: the Scientific Payload, available online at http://sci.esa.int/science-e/www/object/index.cfm?fobjectid=34885, pp. 120–140.

Brace, L. H., Kliore, A. J., 1991. The structure of the Venus ionosphere. Space Sci. Rev. 55, 81–163.

Brace, L. H., Taylor, H. A., Gombosi, T. I., Kliore, A. J., Knudsen, W. C., Nagy, A. F., 1983. The ionosphere of Venus: Observations and their interpretations. In: Hunten, D. M., Colin, L., Donahue, T. M., Moroz, V. I. (Eds.), Venus. Univ. Arizona Press, Arizona, pp. 779–840.

Brain, D. A., 2006. Mars Global Surveyor measurements of the martian solar wind interaction. Space Sci. Rev. 126, 77–112.

Brain, D. A., Lillis, R. J., Mitchell, D. L., Halekas, J. S., Lin, R. P., 2007. Electron pitch angle distributions as indicators of magnetic field topology near Mars. J. Geophys. Res. 112, A09201, 10.1029/2007JA012435.

Cravens, T. E., 2004. Physics of solar system plasmas. Cambridge University Press, New York.

Cravens, T. E., Yelle, R. V., Wahlund, J.-E., Shemansky, D. E., Nagy, A. F., 2010. Composition and structure of the ionosphere and thermosphere. In:

Brown, R. H., Lebreton, J.-P., Waite, J. H. (Eds.), Titan from Cassini-Huygens. Cambridge University Press, pp. 259–296.

Crider, D., Cloutier, P., Law, C., Walker, P., Chen, Y., Acuña, M., Connerney, J., Mitchell, D., Lin, R., Anderson, K., Carlson, C., McFadden, J., Rème, H., Mazelle, C., d'Uston, C., Sauvaud, J., Vignes, D., Brain, D., Ness, N., 2000. Evidence of electron impact ionization in the magnetic pileup boundary of Mars. Geophys. Res. Lett. 27, 45–48.

Crider, D. H., Vignes, D., Krymskii, A. M., Breus, T. K., Ness, N. F., Mitchell, D. L., Slavin, J. A., Acuña, M. H., 2003. A proxy for determining solar wind dynamic pressure at Mars using Mars Global Surveyor data. J. Geophys. Res. 108, 1461, 10.1029/2003JA009875.

Dubinin, E., Fränz, M., Woch, J., Roussos, E., Barabash, S., Lundin, R., Winningham, J. D., Frahm, R. A., Acuña, M., 2006. Plasma Morphology at Mars. Aspera-3 Observations. Space Sci. Rev. 126, 209–238.

Duru, F., Gurnett, D. A., Frahm, R. A., Winningham, J. D., Morgan, D. D., Howes, G. G., 2009. Steep, transient density gradients in the Martian ionosphere similar to the ionopause at Venus. J. Geophys. Res. 114, A12310, 10.1029/2009JA014711.

Duru, F., Gurnett, D. A., Morgan, D. D., Modolo, R., Nagy, A. F., Najib, D., 2008. Electron densities in the upper ionosphere of Mars from the excitation of electron plasma oscillations. J. Geophys. Res. 113, A07302, 10.1029/2008JA013073.

Edberg, N. J. T., Auster, U., Barabash, S., Bößwetter, A., Brain, D. A., Burch, J. L., Carr, C. M., Cowley, S. W. H., Cupido, E., Duru, F., Eriksson, A. I., Fränz, M., Glassmeier, K.-H., Goldstein, R., Lester, M., Lundin, R., Modolo, R., Nilsson, H., Richter, I., Samara, M., Trotignon, J. G., 2009. Rosetta and Mars Express observations of the influence of high solar wind pressure on

the Martian plasma environment. Ann. Geophys. 27, 4533–4545.

Edberg, N. J. T., Nilsson, H., Williams, A. O., Lester, M., Milan, S. E., Cowley, S. W. H., Fränz, M., Barabash, S., Futaana, Y., 2010. Pumping out the atmosphere of Mars through solar wind pressure pulses. Geophys. Res. Lett. 37, L03107, 10.1029/2009GL041814.

Fox, J. L., Dalgarno, A., 1979. Ionization, luminosity, and heating of the upper atmosphere of Mars. J. Geophys. Res. 84, 7315–7333.

Gurnett, D. A., Huff, R. L., Morgan, D. D., Persoon, A. M., Averkamp, T. F., Kirchner, D. L., Duru, F., Akalin, F., Kopf, A. J., Nielsen, E., Safaeinili, A., Plaut, J. J., Picardi, G., 2008. An overview of radar soundings of the martian ionosphere from the Mars Express spacecraft. Adv. Space Res. 41, 1335–1346.

Gurnett, D. A., Kirchner, D. L., Huff, R. L., Morgan, D. D., Persoon, A. M., Averkamp, T. F., Duru, F., Nielsen, E., Safaeinili, A., Plaut, J. J., Picardi, G., 2005. Radar soundings of the ionosphere of Mars. Science 310, 1929–1933.

Kaneda, K., Terada, N., Machida, S., 2007. Time variation of nonthermal escape of oxygen from Mars after solar wind dynamic pressure enhancement. Geophys. Res. Lett. 34, L20201, 10.1029/2007GL030576.

Lillis, R. J., Brain, D. A., 2013. Nightside electron precipitation at Mars: Geographic variability and dependence on solar wind conditions. J. Geophys. Res. 118, 3546–3556.

Luhmann, J. G., Tatrallyay, M., Pepin, R. O., 1992. Venus and Mars: Atmospheres, ionospheres, and solar wind interactions. American Geophysical Union Geophysical Monograph Series.

Luhmann, J. G., Ulusen, D., Ledvina, S. A., Mandt, K., Magee, B., Waite, J. H., Westlake, J., Cravens, T. E., Robertson, I., Edberg, N., Agren, K.,

Wahlund, J.-E., Ma, Y.-J., Wei, H., Russell, C. T., Dougherty, M. K., 2012. Investigating magnetospheric interaction effects on Titan's ionosphere with the Cassini orbiter Ion Neutral Mass Spectrometer, Langmuir Probe and magnetometer observations during targeted flybys. Icarus 219, 534–555.

Lundin, R., Barabash, S., Fedorov, A., Holmström, M., Nilsson, H., Sauvaud, J.-A., Yamauchi, M., 2008. Solar forcing and planetary ion escape from Mars. Geophys. Res. Lett. 35, L09203, 10.1029/2007GL032884.

Ma, Y. J., Fang, X., Nagy, A. F., Russell, C. T., Toth, G., 2014. Martian ionospheric responses to dynamic pressure enhancements in the solar wind. J. Geophys. Res. 119, 1272–1286.

Mantas, G. P., Hanson, W. B., 1979. Photoelectron fluxes in the Martian ionosphere. J. Geophys. Res. 84, 369–385.

Mitchell, D. L., Lin, R. P., Mazelle, C., Rème, H., Cloutier, P. A., Connerney, J. E. P., Acuña, M. H., Ness, N. F., 2001. Probing Mars' crustal magnetic field and ionosphere with the MGS Electron Reflectometer. J. Geophys. Res. 106, 23419–23428.

Mitchell, D. L., Lin, R. P., Rème, H., Crider, D. H., Cloutier, P. A., Connerney, J. E. P., Acuña, M. H., Ness, N. F., 2000. Oxygen Auger electrons observed in Mars' ionosphere. Geophys. Res. Lett. 27, 1871–1874.

Nagy, A. F., Winterhalter, D., Sauer, K., Cravens, T. E., Brecht, S., Mazelle, C., Crider, D., Kallio, E., Zakharov, A., Dubinin, E., Verigin, M., Kotova, G., Axford, W. I., Bertucci, C., Trotignon, J. G., 2004. The plasma environment of Mars. Space Sci. Rev. 111, 33–114.

Nilsson, H., Carlsson, E., Brain, D. A., Yamauchi, M., Holmström, M., Barabash, S., Lundin, R., Futaana, Y., 2010. Ion escape from Mars as a function of solar wind conditions: A statistical study. Icarus 206, 40–49.

Opgenoorth, H. J., Andrews, D. J., Fränz, M., Lester, M., Edberg, N. J. T.,

Morgan, D., Duru, F., Witasse, O., Williams, A. O., 2013. Mars ionospheric response to solar wind variability. J. Geophys. Res. 118, 6558–6587.

Opitz, A., Fedorov, A., Wurz, P., Szego, K., Sauvaud, J.-A., Karrer, R., Galvin, A. B., Barabash, S., Ipavich, F., 2010. Solar-wind bulk velocity throughout the inner heliosphere from multi-spacecraft measurements. Solar Phys. 264, 377–382.

Opitz, A., Karrer, R., Wurz, P., Galvin, A. B., Bochsler, P., Blush, L. M., Daoudi, H., Ellis, L., Farrugia, C. J., Giammanco, C., Kistler, L. M., Klecker, B., Kucharek, H., Lee, M. A., Möbius, E., Popecki, M., Sigrist, M., Simunac, K., Singer, K., Thompson, B., Wimmer-Schweingruber, R. F., 2009. Temporal evolution of the solar wind bulk velocity at solar minimum by correlating the STEREO A and B PLASTIC measurements. Solar Phys. 256, 365–377.

Pätzold, M., Neubauer, F. M., Carone, L., Hagermann, A., Stanzel, C., Häusler, B., Remus, S., Selle, J., Hagl, D., Hinson, D. P., Simpson, R. A., Tyler, G. L., Asmar, S. W., Axford, W. I., Hagfors, T., Barriot, J.-P., Cerisier, J.-C., Imamura, T., Oyama, K.-I., Janle, P., Kirchengast, G., Dehant, V., 2004. MaRS: Mars Express Orbiter Radio Science. ESA SP-1240: Mars Express: the Scientific Payload, available online at http://sci.esa.int/science-e/www/object/index.cfm?fobjectid=34885, pp. 141–163.

Pätzold, M., thirty colleagues, 2009. MaRS: Mars Express Radio Science Experiment. ESA SP-1291: Mars Express: the Scientific Investigations, available online at http://sci.esa.int/science-e/www/object/index.cfm?fobjectid=47218, pp. 217–245.

Peter, K., Pätzold, M., Molina-Cuberos, G., Witasse, O., González-Galindo, F., Withers, P., Bird, M. K., Häusler, B., Hinson, D. P., Tellmann, S., Tyler,

G. L., 2014. The dayside ionospheres of Mars and Venus: Comparing a one-dimensional photochemical model with MaRS (Mars Express) and VeRa (Venus Express) observations. Icarus 233, 66–82.

Russell, C. T., 2006. Foreword. Space Sci. Rev. 126, 1–4.

Russell, C. T., Vaisberg, O., 1983. The interaction of the solar wind with Venus. In: Hunten, D. M., Colin, L., Donahue, T. M., Moroz, V. I. (Eds.), Venus. Univ. Arizona Press, Arizona, pp. 873–940.

Schunk, R. W., Nagy, A. F., 2009. Ionospheres, second edition. Cambridge Univ. Press, New York.

Vignes, D., Mazelle, C., Rème, H., Acuña, M. H., Connerney, J. E. P., Lin, R. P., Mitchell, D. L., Cloutier, P., Crider, D. H., Ness, N. F., 2000. The solar wind interaction with Mars: Locations and shapes of the bow shock and the magnetic pile-up boundary from the observations of the MAG/ER Experiment onboard Mars Global Surveyor. Geophys. Res. Lett. 27, 49–52.

Witasse, O., Cravens, T., Mendillo, M., Moses, J., Kliore, A., Nagy, A. F., Breus, T., 2008. Solar system ionospheres. Space Sci. Rev. 139, 235–265.

Withers, P., 2009. A review of observed variability in the dayside ionosphere of Mars. Adv. Space Res. 44, 277–307.

Withers, P., Fallows, K., Girazian, Z., Matta, M., Häusler, B., Hinson, D., Tyler, L., Morgan, D., Pätzold, M., Peter, K., Tellmann, S., Peralta, J., Witasse, O., 2012. A clear view of the multifaceted dayside ionosphere of Mars. Geophys. Res. Lett. 39, L18202, 10.1029/2012GL053193.

Zhang, M. H. G., Luhmann, J. G., 1992. Comparisons of peak ionosphere pressures at Mars and Venus with incident solar wind dynamic pressure. J. Geophys. Res. 97, 1017–1025.

Zhang, M. H. G., Luhmann, J. G., Kliore, A. J., Kim, J., 1990. A post-Pioneer Venus reassessment of the martian dayside ionosphere as observed by radio

occultation methods. J. Geophys. Res. 95, 14829–14839.

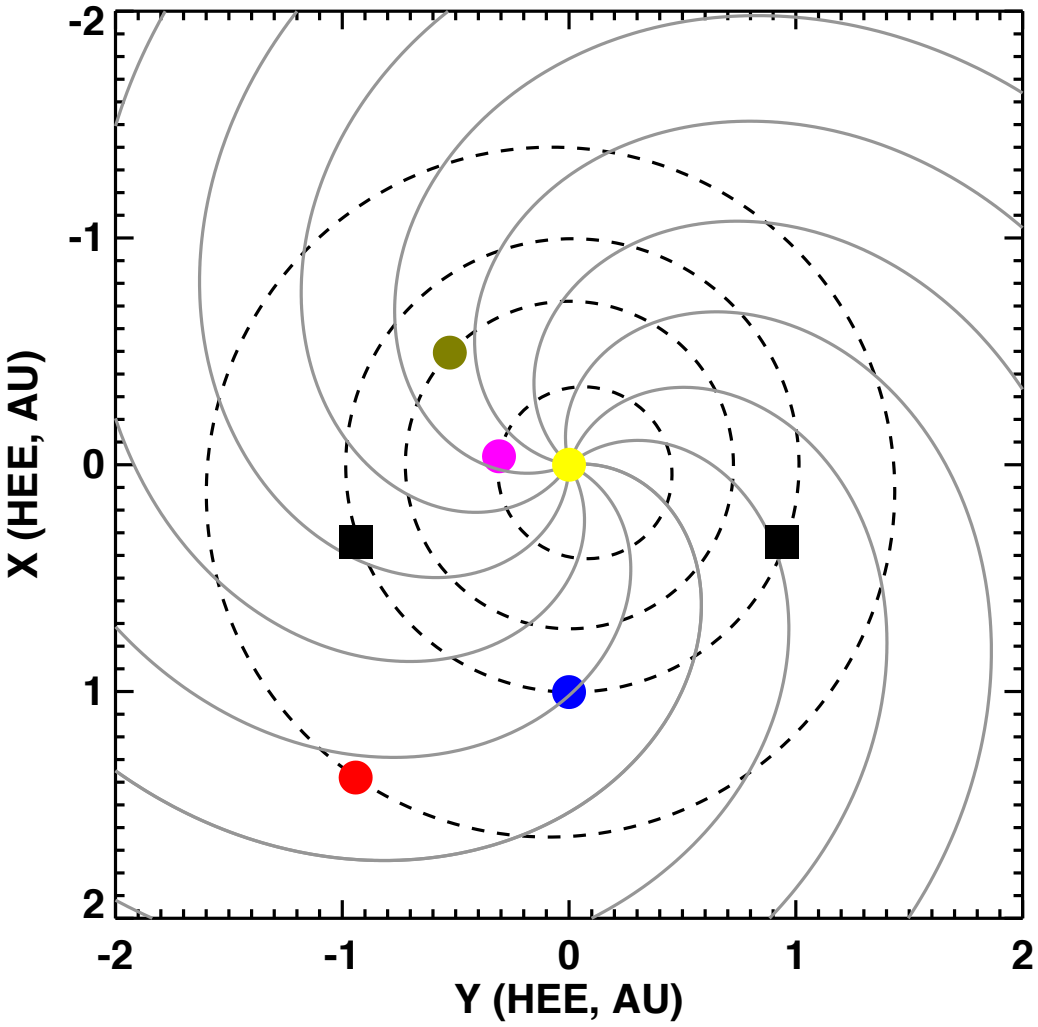

Fig. 1. Positions of Earth and Mars on 1 April 2010. The Sun, Mercury, Venus, and STEREO-A (right square) and -B (left square) are also shown. Coordinates are given in the Heliocentric Earth Equatorial system in units of AU. The Parker spiral structure of the solar wind (400 km s^{-1}) is also illustrated.

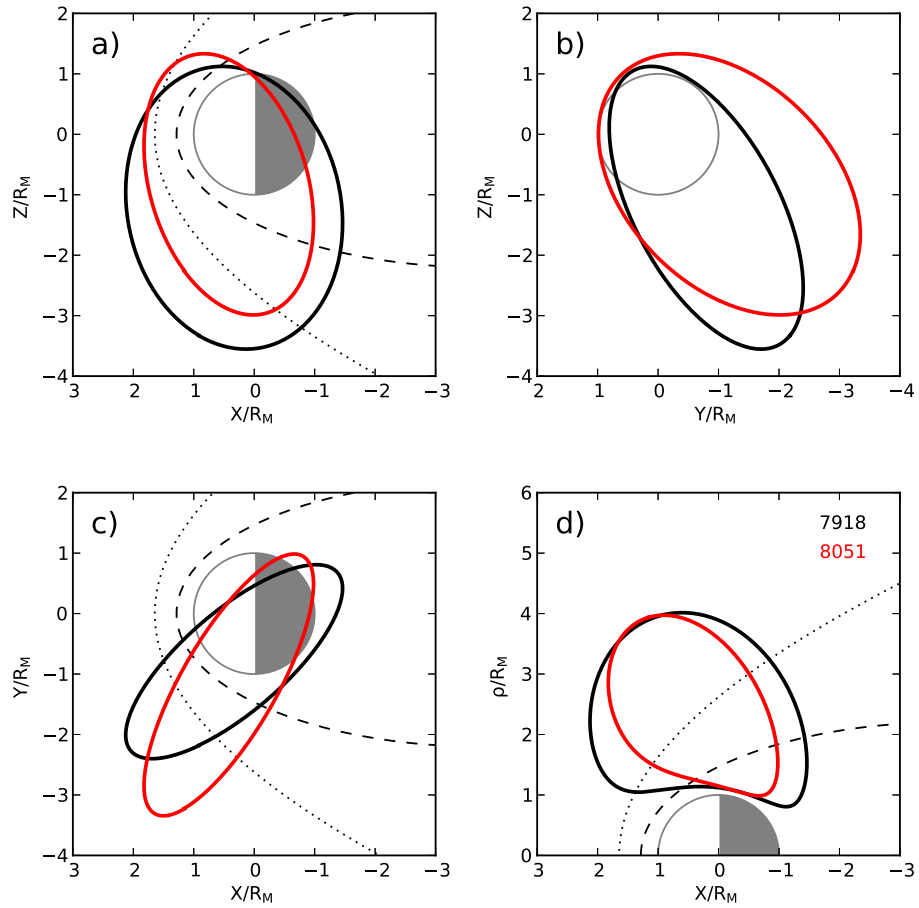

Fig. 2. MEX orbit geometry for 7 March (orbit 7918, black) and 15 April (orbit 8051, red) in Mars-centered Solar Orbital (MSO) coordinates. Modelled positions of the magnetic pile up boundary and the bow shock, according to Vignes et al. (2000), are also shown. Panel A shows the XZ plane, Panel B shows the YZ plane, and Panel C shows the XY plane. Panel D shows a cylindrical representation in which $\rho^2 = \mathrm{Y}^2 + \mathrm{Z}^2$.

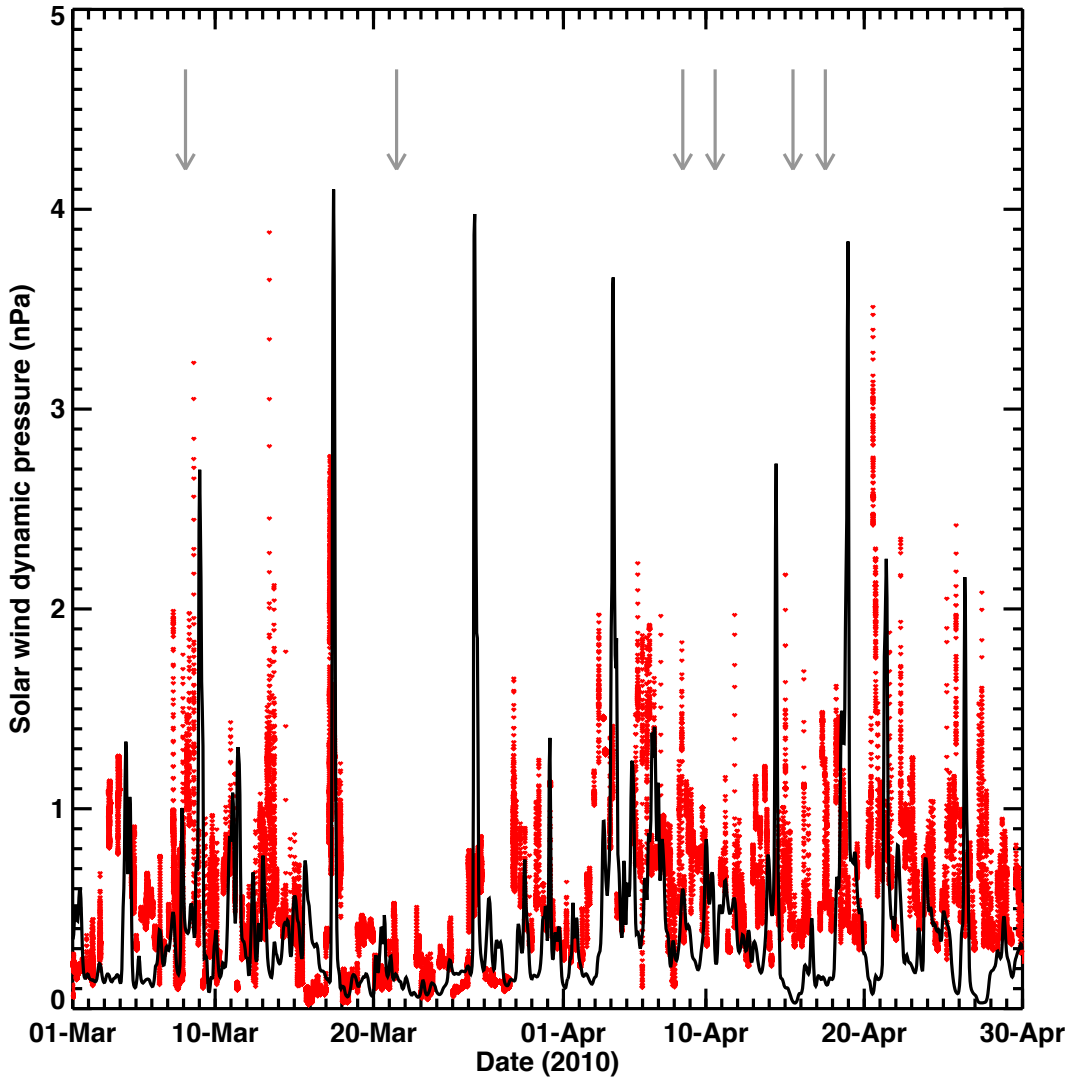

Fig. 3. Solar wind dynamic pressure measured at Mars by ASPERA (red) and extrapolated to Mars from STEREO-B (black). Grey arrows mark the times of the six radio occultations (Section 4.1).

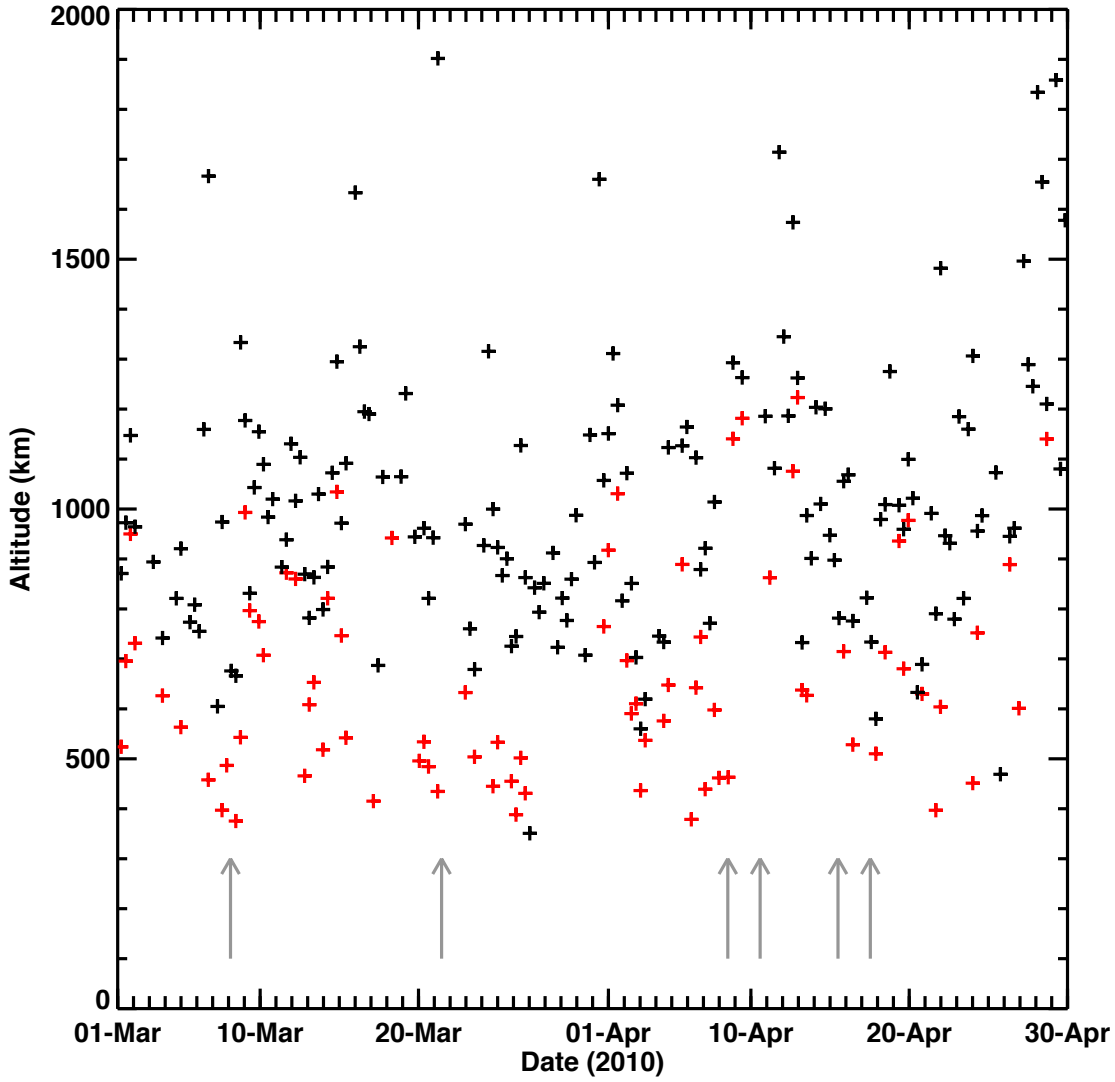

Fig. 4. Altitudes of the photoelectron boundary (red) and magnetic pileup boundary (black) on the outbound leg of the MEX orbit. Grey arrows mark the times of the six radio occultations (Section 4.1).

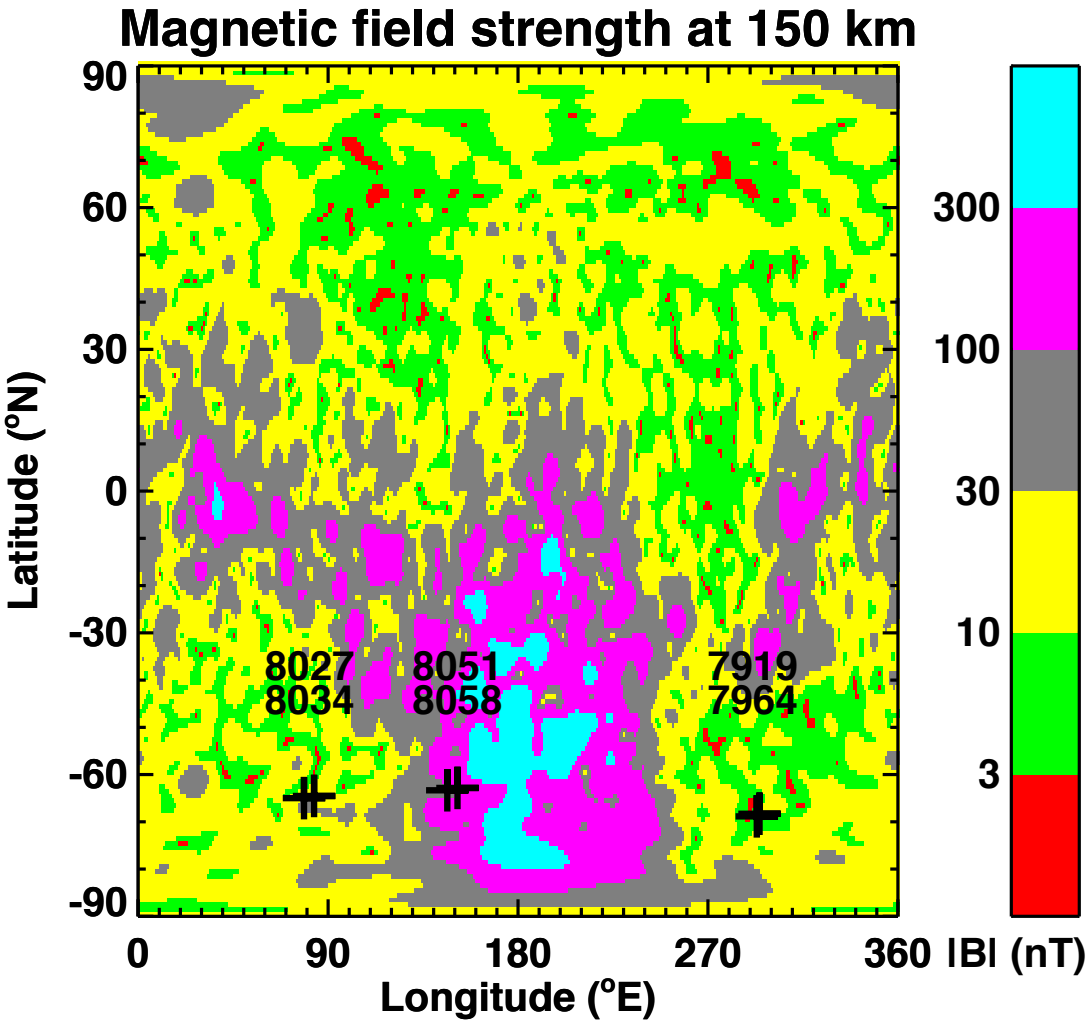

Fig. 5. Locations of six MEX radio occultation profiles (crosses). Pairs of numbers indicate the orbit numbers of each occultation. Also shown is the magnetic field strength at 150 km based upon the model of Arkani-Hamed (2004).

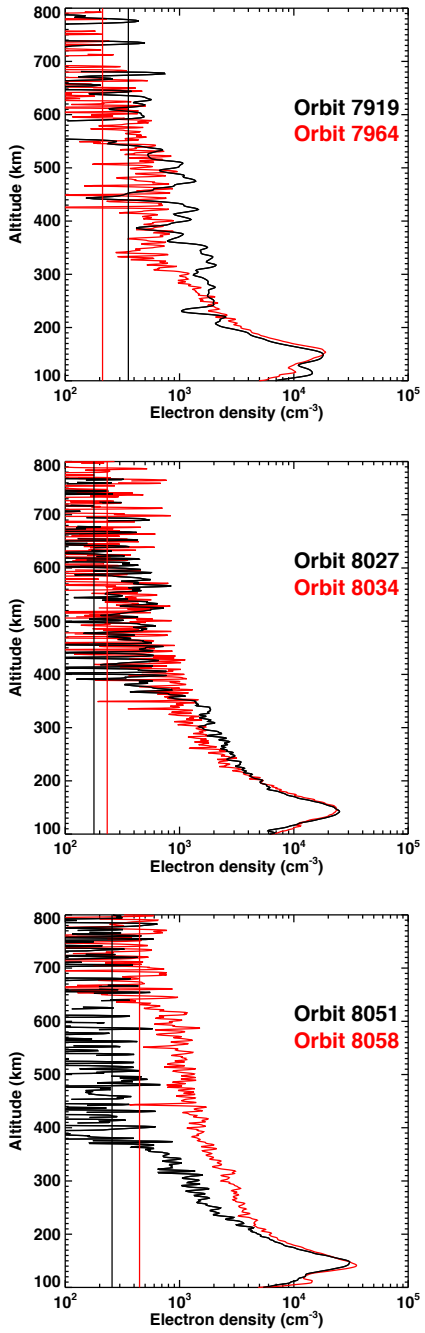

Fig. 6. Top. Smoothed radio occultation electron density profiles from 8 March (orbit 7919, black) and 21 March (orbit 7964, red). Black and red vertical lines indicate the 1σ uncertainty in electron density for the corresponding profile. Middle. As top panel, but 8 April (orbit 8027, black) and 10 April (orbit 8034, red). Bottom. As top panel, but 15 April (orbit 8051, black) and 17 April (orbit 8058, red).

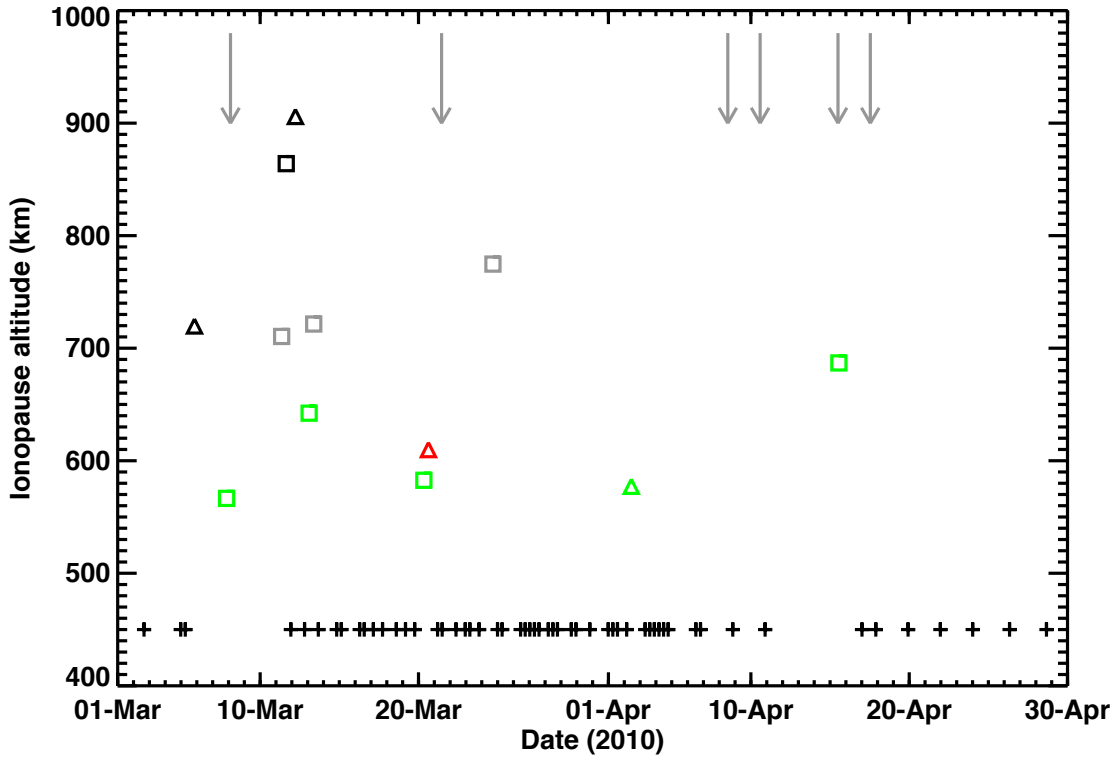

Fig. 7. Altitudes of abrupt changes in electron density detected in MARSIS local electron density data in March/April 2010. More abrupt changes, or those that would be classified as "ionopause" detections by Duru et al. (2009), are shown by squares and less abrupt changes are shown by triangles. Colour indicates SZA: 65°–70° as black, 70°–75° as grey, 75°–80° as red, and 80°–85° as green. Orbits on which no abrupt change was detected are shown as black crosses at 450 km. Grey arrows mark the times of the six radio occultations (Section 4.1).

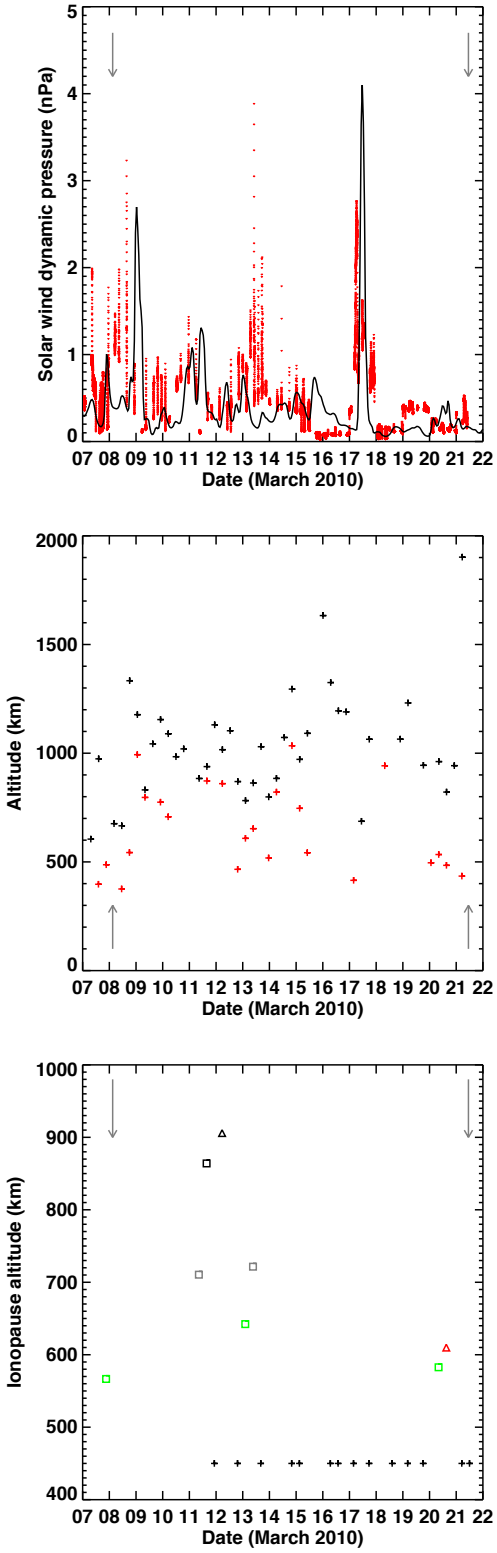

Fig. 8. Properties of the solar wind (top), magnetic pileup boundary and photoelectron boundary (middle), and ionopause (bottom) for a period centered on case study A. Data and symbols for each panel as in Figures 3, 4, and 7.

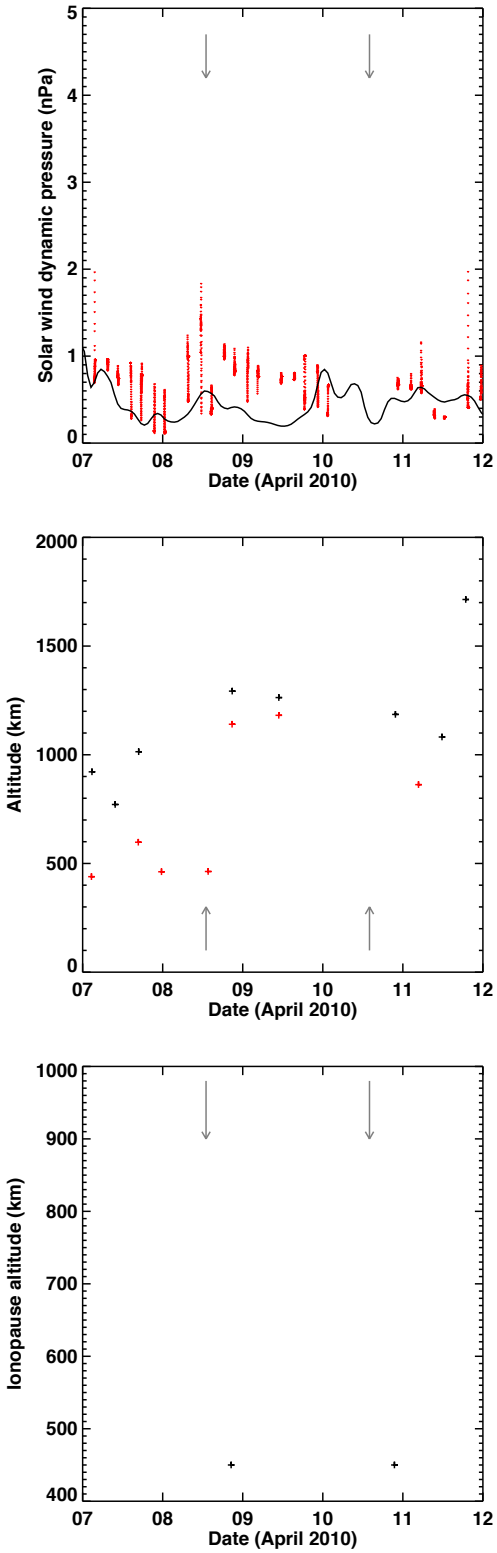

Fig. 9. As Figure 8, but for case study B.

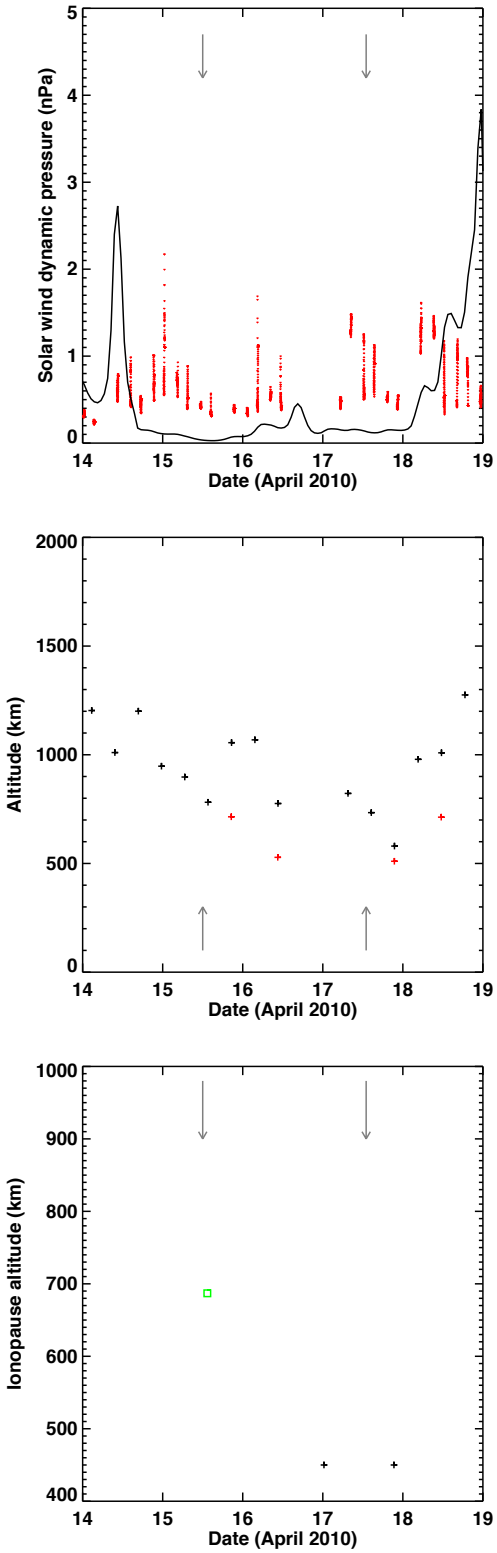

Fig. 10. As Figure 8, but for case study C.

Table 1

Details of the six radio occultation profiles used in this work

Date and time (UTC)	Day of year	Latitude (°N)	Longitude (°E)	SZA (deg)	Orbit
2010-03-08T03:27:02.692	67	-69.14	292.24	93.68	7919
2010-03-21T11:25:08.136	80	-68.62	293.45	93.37	7964
2010-04-08T13:03:21.582	98	-65.49	77.37	91.05	8027
2010-04-10T14:01:12.242	100	-65.05	82.12	90.70	8034
2010-04-15T12:56:13.638	105	-63.93	145.17	89.78	8051
2010-04-17T13:54:16.250	107	-63.46	149.97	89.38	8058